Inverse Abel transform algorithms to determine the radial profile of the photoelastic coefficient of glass optical fibers

Acheroy, S.; Merken, P.; Geernaert, Thomas; Ottevaere, Heidi; Thienpont, Hugo; Berghmans, Francis

Published in:
Optical Sensing and Detection IV

DOI:
10.1117/12.2227755

Publication date:
2016

Document Version:
Final published version

Inverse Abel transform algorithms to determine the radial profile of the photoelastic coefficient of glass optical fibers

Sophie Acheroy*[a], Patrick Merken[a], Thomas Geernaert[b], Heidi Ottevaere[b], Hugo Thienpont, Francis Berghmans[b]

[a]Royal Military Academy, Dept of Communication, Information, Systems and Sensors (CISS), Ave Renaissance 30, 1000 Brussels, Belgium; [b]Vrije Universiteit Brussel, Dept. of Applied Physics and Photonics, Brussels Photonics Team (B-PHOT), Pleinlaan 2, B-1050 Brussels, Belgium

ABSTRACT

We compare two algorithms to determine the radial profile of the photoelastic coefficient C in glass optical fibers. We first measure the retardance profile of a transversally illuminated fiber as a function of tensile load. The radial profile C(r) is obtained from the inverse Abel transform of this retardance profile. Our first algorithm expands the measured retardance in its Fourier coefficients before computing the inverse Abel transform. With the second algorithm the expected result of the inverse Abel transform is expanded and the forward Abel transform of that expansion is compared to the measured retardance. We apply both approaches on the retardance measurement of commercially available single mode and multi-mode fibers.

Keywords: Photoelastic coefficient, fiber optic characterization, inverse Abel transform

1. INTRODUCTION

Fiber optic sensors are increasingly used in many applications. Such sensors usually exploit the photoelastic effect for measuring mechanical quantities such as strain, stress, pressure or transverse load [1–4]. Accurately predicting the response of an optical fiber sensor to mechanical load therefore requires good knowledge of the material parameters of the fiber, such as the photoelastic coefficient C [Pa^{-1}] which links the applied load to the change of the refractive index in the fiber. The measurement and analysis techniques proposed in literature rely on the hypothesis that C is constant over the fiber cross-section [5,6] but this is not straightforward taking into account the particular fabrication process of glass fibers. The purpose of this manuscript is therefore to describe a measurement method to determine the radial distribution of C(r) along the fiber section, with r the radial distance from the center of the fiber. The determination of C(r) requires first to measure the retardance profile R(y) of a transversally illuminated fiber as a function of the tensile load applied to the fiber, where y is taken perpendicularly to the projected fiber axis [7–9]. The inverse Abel transform of R(y) allows obtaining the radial profile of C(r). The inverse Abel transform involves integrating the derivative of R(y), which implies that measurement noise on R(y) significantly impacts the final result. We propose two methods to compute the inverse Abel transform of the retardance profile. Both use Fourier theory. In the first algorithm we expand R(y) in Fourier series and compute the inverse Abel transform to obtain C(r) based on [10]. For the second algorithm, we propose to expand the expected result C(r) in Fourier series and compute the forward Abel transform to obtain the measured retardance [11]. To compare the behavior and convergence of both algorithms we apply them to a known theoretical profile with added Gaussian noise. Finally we use both algorithms to determine the radial profile of C(r) in glass fibers. The measurement method and the two proposed inverse Abel transform algorithms are discussed in section 2. In section 3 we present and discuss the results of the radial profile measurement of the photoelastic coefficient of the tested fibers.

2. MEASUREMENT METHOD AND ALGORITHMS

2.1 Determination of the retardance

A detailed description of the measurement method that we use to determine the radial distribution of the photoelastic constant C(r) in an optical fiber is available in previous work [9,12]. We shortly recall the measurement principle below for sake of completeness. Figure 1 shows the Cartesian axes system, in which we take the z-axis along the fiber axis. The fiber is subjected to a known axial stress σ_z which we assume to be constant across the fiber section. Monochromatic

Optical Sensing and Detection IV, edited by Francis Berghmans, Anna G. Mignani, Proc. of SPIE
Vol. 9899, 98992F · © 2016 SPIE · CCC code: 0277-786X/16/$18 · doi: 10.1117/12.2227755

light at 633 nm and linearly polarized at 45°C in the yz-plane illuminates the fiber. As illustrated in Figure 1 the wave vector of the light is perpendicular to the fiber axis and parallel with the x-axis. The fiber is immersed in index matching liquid to avoid that the wave vector changes direction at the boundaries of the optical fiber.

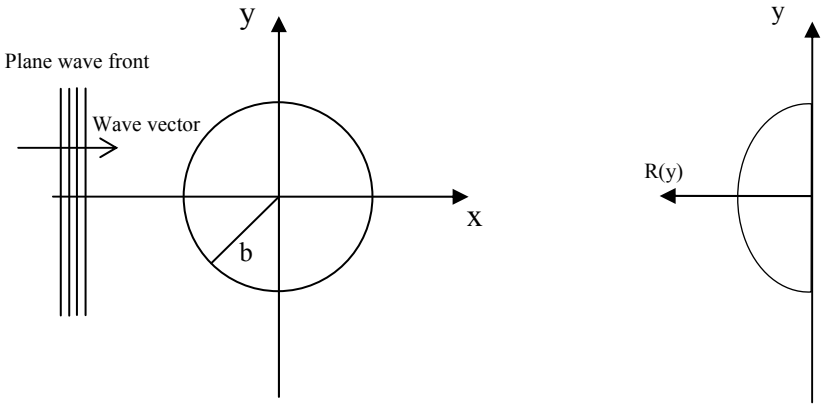

Figure 1: Illustration of an optical fiber transversely illuminated with a plane wave (left) and resulting retardance profile R(y) (right). b is the radius of the fiber. The z-axis is taken along the fiber length with a direction exiting the page.

The axial load applied to the fiber induces birefringence in the fiber material. The two linearly polarized components along the y and z directions will experience a different phase shift that can be observed as the projected retardance R(y) between these two orthogonal components. The projected retardance R(y) is related to the axial stress by an inverse Abel transform [7,13,14], as given by equation (1):

$$C(r).\sigma_z = -\frac{1}{\pi}\int_r^b \frac{dR(y)/dy}{\sqrt{y^2 - r^2}}dy \tag{1}$$

The photo-elastic constant C(r) is the regression coefficient linking the inverse Abel transform of the projected retardance R(y) and the applied known axial stress σ_z. r is the radial distance taken from the fiber's center and b is the radius of the fiber. To obtain the radial profile of the photoelastic constant C(r), we use a polarizing microscope and apply the Sénarmont compensation method to measure the full-field view of the retardance R(y).

2.2 Original inverse Abel transform algorithm

Once we have measured R(y) we still have to determine its inverse Abel transform to obtain the radial profile of the photoelastic constant. The first algorithm we propose, referred to as 'A1' relies on the Fourier theory described in [15,16]. The measured retardance R(y) is expanded in Fourier series and the inverse Abel transform of the retardance is computed with equation (2).

$$C(r).\sigma_z = -\frac{\pi}{2b}\sum_{k=1}^{k\max} a_k k \frac{2}{\pi}\int_0^{\sqrt{1-\rho^2}} (t^2+\rho^2)^{-1/2} \times \sin(k\pi\sqrt{t^2+\rho^2})dt \tag{2}$$

where $\rho = r/b$ is the normalized radius, $t = \sqrt{1-\rho^2}$ and a_k is the kth Fourier coefficient of the Fourier series of the retardance. The inverse Abel transform requires the integration of the derivative of R(y) which means that the measurement noise has a significant impact on the final result. Increased measurement noise leads to a larger variance of the final profile of the photoelastic coefficient. This prompted us to seek for improvement of our algorithm.

2.3 Adapted inverse Abel transform algorithm

The new algorithm, referred to as 'A2', still relies on the Fourier theory. However, instead of expanding the measured retardance R(y) in Fourier series, we expand the product $C(r).\sigma_z$ as described in [17]. With this approach, the forward Abel transform of $C(r).\sigma_z$ has to be applied to obtain the measured retardance. The advantage of the forward Abel transform is that is does not involve the integration of a derivative. This new algorithm should lead to results with a lower variance than those we obtain with A1. Furthermore, there is a constant term in the Fourier expansion of $C(r).\sigma_z$ what we expect to quicken the convergence. With A1 the retardance R(y) is expanded and the inverse Abel transform of R(y) requires deriving R(y). Consequently the constant term disappears and a higher number of Fourier coefficients are required to allow A1 to converge towards a stable profile. Additional coefficients are not an issue when dealing with stable retardance measurements, but can be problematic if the measurement is noisy. We thus expect a better and more robust behavior of A2 when dealing with noisy data. The expansion of $C(r).\sigma_z$ is shown in equation (3).

$$\left[C(r).\sigma_z\right]_F = a_0 + \sum_{k=1}^{\infty} a_k \cos(k\pi \frac{r}{b}) \tag{3}$$

a_k is the kth Fourier coefficient of the expansion. Note that any cosine function can be used to implement the Fourier expansion without affecting the final result. To obtain the computed retardance $R_F(y)$ from the product $\left[C(r).\sigma_z\right]_F$ we now have to calculate the forward Abel transform of the latter. The analytical expression of the forward Abel transform is given by equation (4)

$$R(y) = 2\int_y^b \left[C(r)\sigma_z\right]_F \frac{r}{\sqrt{r^2 - y^2}} dr \tag{4}$$

Substituting equation (3) in equation (4) yields the final expression of the retardance, which can be written as equation (5).

$$R_F(y) = b.a_0 \int_0^{\sqrt{1-\rho^2}} dt + b\sum_{k=1}^{\infty} a_k \int_0^{\sqrt{1-\rho^2}} \cos(k\pi\sqrt{t^2+\rho^2})dt \tag{5}$$

where $\rho = x/b$ is the normalized radius and $t = \frac{\sqrt{r^2 - y^2}}{b}$.

The last step is the determination of $R_F(y)$ that is fully defined by the Fourier coefficients a_k. To compute the magnitude of these coefficients we apply the least square criterion [18] and we evaluate the expression given in equation (6).

$$\sum_i^N \left[R_F(y_i) - R(y_i)\right]^2 \overset{!}{=} Min \tag{6}$$

2.4 Comparison and evaluation of both algorithms

To compare the performance of the two algorithms we take R(y) equal to a half an ellipse E(y). Assuming that tensile stress and C are constant across the fiber, the shape of the retardance profile should indeed be elliptical. The analytical expression of the inverse Abel transform of the semi-ellipse is a constant value that depends on the semi-long and semi-short axis of the ellipse (see equation (7)).

$$IAT\left[E(y) = -\mathrm{A}^2\sqrt{1+\frac{y^2}{B^2}}\right] = -\frac{1}{2}\frac{A}{B} \tag{7}$$

We apply both algorithms in two steps. First we compare the results on the ellipse without added noise E(y). Figure 2 shows the results of both algorithm on E(y) for a small and a high number of Fourier coefficients, i.e. $k_1 = 10$ and $k_2 = 50$. A1 clearly needs a large amount of Fourier coefficients to converge to the theoretical shape of the inverse Abel transform of E(y).

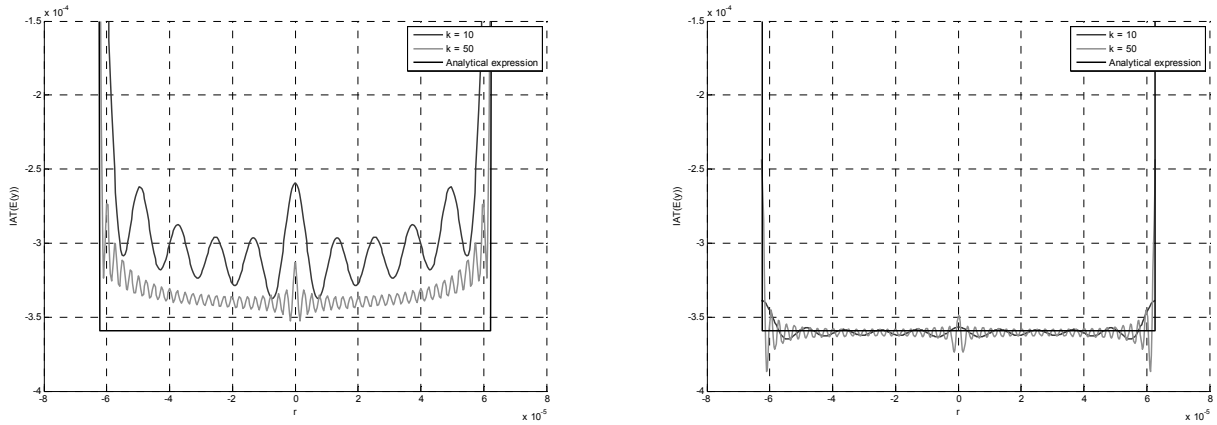

Figure 2: The inverse Abel transform of the half ellipse E(y) computed with A1 (left) and A2 (right). The transform is computed for respectively $k_1 = 10$ and $k_2 = 50$ Fourier coefficients and compared to the analytical expression of the inverse transform of E(y).

In a second step we compute the inverse Abel transform of E(y) with added Gaussian noise to simulate real measurements. The standard deviation of the Gaussian noise is fixed to 1.0×10^{-9} nm, to correspond to the actual standard deviation of measured noisy retardances.A1 requires a higher amount of Fourier coefficients to get close to the analytical expression of the inverse Abel transform. While it has no incidence when we apply the algorithm on E(y), it goes at the expense of a very noisy profile when we consider the inverse Abel transform of the ellipse with added Gaussian noise, as illustrated in Figure **3**.

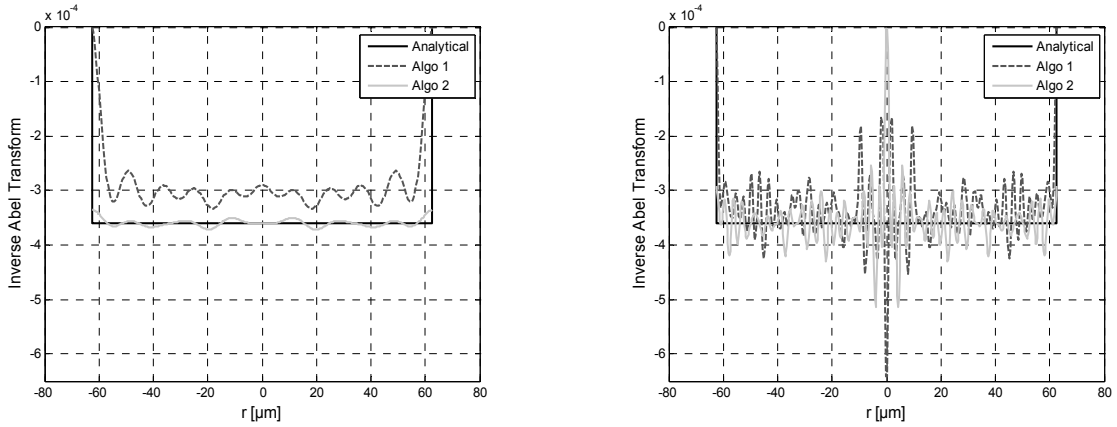

Figure 3: The inverse Abel transform of the noisy ellipse for $k_1 = 10$ (left) and $k_2 = 50$ (right) computed with A1 and A2. The standard deviation of the Gaussian noise on top of the signal is 1.0×10^{-9} nm. The results are compared to the analytical value of the inverse transform of E(y).

Additionally, to quantify and compare the performance of both algorithms we consider the root-mean-square error (RMSE) between the analytical expression of the inverse Abel transform and the computed inverse Abel transform of the perfect and noisy ellipse for a range of Fourier coefficients from k = 1 to k = 200. We calculate the average error as a function of k. In Figure 4 we present the results of that comparison. In our previous publication [8] we describe in detail

the methodology to obtain the RMSE and we concluded that a higher number of Fourier coefficients leads to a better results..

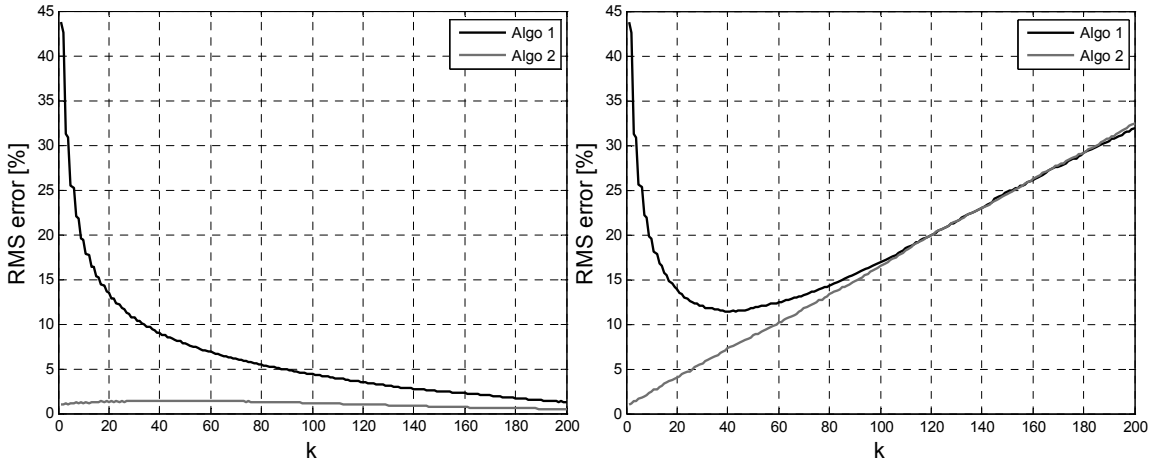

Figure 4: RMSE between the analytical value of the inverse Abel transform of the ellipse and the computed Abel transform of E(y) without added noise on the left and of noisy ellipse on the right as a function of the amount of Fourier coefficients k. The standard deviation of the Gaussian noise added to E(y) is $\sigma = 0.1 \times 10^{-9}$ nm.

The graph at the left in Figure 4 shows that the RMSE for both algorithms reduces with a high number of Fourier coefficients, but A2 converges faster than A1. However, when the variance of the Gaussian noise increases, the influence of the noise on the inverse Abel transform becomes predominant and a high number of Fourier coefficients leads to very noisy shapes. In that case the amount of considered coefficients has to be reduced. The graph at the right in Figure 4 evidences that A2 is more robust than A1 for computing inverse Abel transforms of profiles with a high variance. A minimal error of 12% with A1 requires about 40 coefficients, whilst A2 achieves much lower errors with a small value of k. For an increasing amount of Fourier coefficients both algorithms tend to behave in the same manner with an increasing RMSE.

3. RESULTS AND DISCUSSION

We have determined the radial profile of the photoelastic constant of commercially available single mode and multimode glass optical fibers. The main characteristics of these fibers are summarized in Table 1.

Table 1: Main characteristics of the glass optical fibers used to measure the retardance and determine the radial profile of the photoelastic coefficient [19].

Fiber	Type	Mode	d_{core}	$d_{cladding}$	n_{core}	$n_{cladding}$
1	Ge-doped Silica core	Singlemode	9 µm	125 µm	1,462	1,458
2	F-doped depressed cladding	Multimode	50 µm	125 µm	1,457	1,440
3	F-doped depressed cladding	Multimode	105 µm	125 µm	1,457	1,440

We use two approaches to determine the photoelastic constant C. First the measured retardance is approximated with the shape of a half ellipse and the analytical expression given in equation (7) is used to determine the inverse Abel transform of the retardance. The relation between the axial stress and the retardance becomes:

$$C.\sigma_z = -\frac{1}{2}\frac{\max(abs(R(y)))}{b} \tag{8}$$

b is the fiber radius, R(y) the measured retardance and σ_z the axial stress. C is the regression coefficient that has to be determined. We determine the retardance profile for tensile stress that varies from 82 MPa to 185 MPa. The results we obtain with the approximated method are depicted in Figure 5 for fibers 1 and 3. Fiber 2 has a particular retardance profile

suggesting the fiber is dual-clad with depressed inner cladding [20,21]. Due to the particular index profile, the retardance profile we measure is not at all elliptical. As a consequence we cannot apply the elliptical approximation on this fiber.

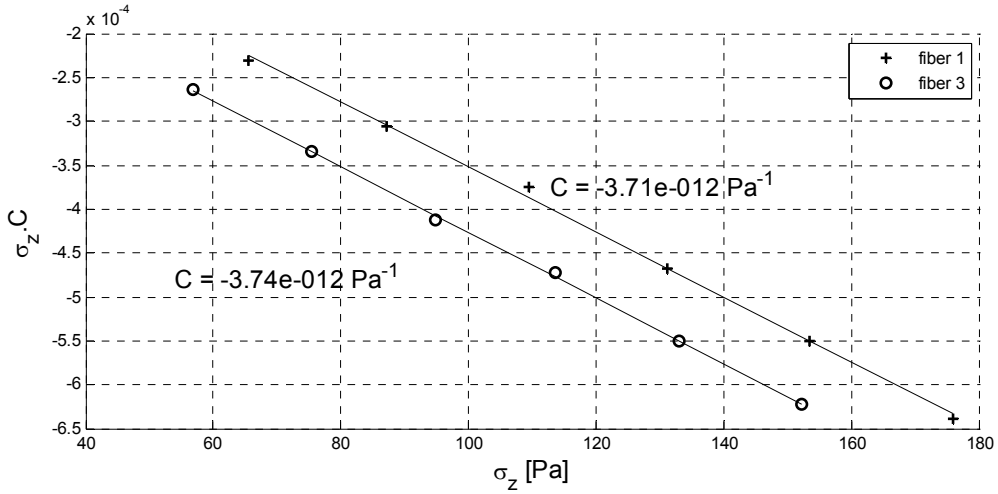

Figure 5: C.σ_z as a function of the axial stress. The regression coefficient is the photoelastic constant C. Its values are indicated in the graph along the respective linear fit.

The elliptical approximation allows determining the mean value of the photoelastic constant. We obtain C values of -3.71×10^{-12} Pa^{-1} and -3.74×10^{-12} Pa^{-1} for the silica glass fibers 1 and 3. This value is slightly higher than the value measured on bulk fused silica (C = -3.52×10^{-12} Pa^{-1}) determined in [22].

In the second approach we determine the radial profile of the photoelastic coefficient without any approximation. We first compute the inverse Abel transform of each measured retardance profile corresponding to a specific tensile stress. We then apply A1 and A2 to determine the inverse Abel transform of the retardance profiles. We obtain the relationship $f(r) = C(r).\sigma_z$.

Working out the linear regression of $f(r)$ for every radial point finally yields the radial distribution of the photoelastic constant C(r). Figure 6 represents the radial profiles of the photoelastic constant for the three different optical fibers. The standard deviation of the retardance measured for glass fiber 1 is small ($\sigma_{glass} < 0.5\times10^{-9}$). The results are similar and confirm that both algorithms behave equivalently for profiles with a low noise level. The difference in refractive index between core and cladding for glass fibers 2 and 3 is four times larger compared to fiber 1. This increases the scattering at the boundaries between the two materials and increases the noise on the measured retardance R(y). The Ge-doped core of fiber 1 does not influence the profile of C(r). From Figure 6 (a) we can conclude that C(r) is constant throughout the cross-section of this fiber. On the other hand, Figure 6 (b) and 6 (c) evidence that the value of C(r) in the fluorine-doped cladding portion differs significantly from the value of C(r) in the undoped core of fiber 2 and 3 and from the outer cladding of fiber 2.

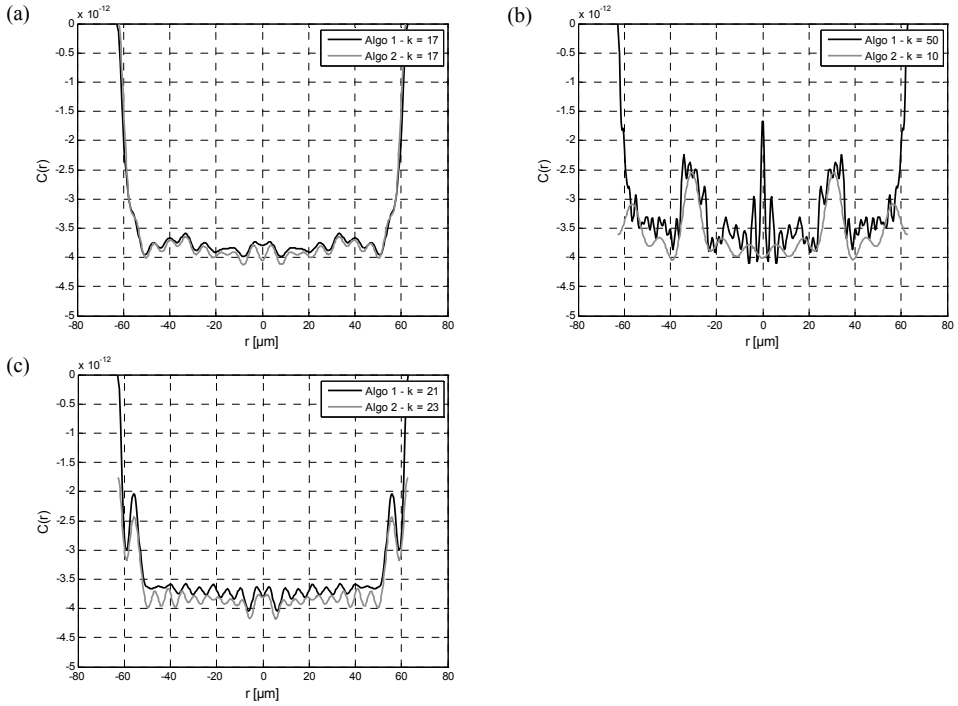

Figure 6: Radial distribution of the photoelastic constant C(r) in one fiber section. The profiles are respectively computed with A1 and A2. (a) C(r) in fiber 1, (b) C(r) in fiber 2 and (c) C(r) in fiber 3. The respective value of k is mentioned in the graph.

In agreement with the conclusions of Section 2, the first algorithm requires a higher number of Fourier coefficients k to achieve a correct profile at the expense of increasing the impact of the measurement noise. For the second algorithm less Fourier coefficients are needed to achieve a reliable and stable result. We also compute the average value of C(r) in the stable parts of the radial profiles and we obtain respectively -3.83×10-12 Pa^{-1}, -3.75×10-12 Pa^{-1} and -3.80×10-12 Pa^{-1} for glass fiber 1 and for the undoped portions of fibers 2 and 3. These figures are comparable with the mean values of the photoelastic constant that we have determined with the elliptical approximation. The mean value of C(r) equals -2.75×10-12 Pa^{-1} in the fluorinated trenches of the cladding. Our results show that the fluorine doping decreases the absolute value of C with about 27% compared to pure silica or Ge-doped silica glass fibers.

4. CONCLUSIONS

We discussed two algorithms to calculate the inverse Abel transform of the retardance, which is required to determine the radial profile of the photoelastic coefficient C in optical fibers. The first algorithm decomposes the measured retardance in its Fourier coefficients and afterwards computes the inverse Abel transform. The second algorithm, on the other hand, starts from the expansion of the desired profile in Fourier series and then computes the forward Abel transform. The obtained function is compared to the measured retardance based on the least squares criterion. In case the retardance profile has a small variance, both algorithms tend to behave the same way. The main difference is the higher amount of Fourier coefficients that has to be taken into account to allow the first algorithm to converge. The most important conclusion here is that the second algorithm is more robust to compute the inverse Abel transform when dealing with noisy measurements.

We have determined C(r) of different silica glass fibers using both algorithms. The mean value of C determined with the elliptical approximation and the average value of C(r) in the stable parts of the profiles are equivalent. The mean value of C computed for the three fibers under test equals -3.78×10^{-12} Pa^{-1} in the undoped and Ge-doped portions of the cross-sections. The average value of C in the fluorine-doped part of the cladding region is 27% smaller. With respect to the radial distribution of C(r), we conclude that the photoelastic coefficient can be considered constant throughout the fiber section for silica fibers that only conclude a Ge-doped core. This is no longer the case in silica glass fibers containing a fluorine-doped depressed cladding.

REFERENCES

[1] K. Peeters, "Polymer optical fibre sensors - A review," *Smart Mater. Struct.* **20**(013002), IOP Publishing (2011) [doi:10.1088/0964-1726/20/1/013002].

[2] F. Berghmans and H. Thienpont, "Plastic Optical Fibers for Sensing Applications," 3–5 (2014).

[3] A. D. Kersey and M. A. Davis, "Fiber grating sensors," *J. Light. Technol.* **15**(8), 1442–1463 (1997).

[4] D. J. Webb, "Fibre Bragg grating sensors in polymer optical fibres," *Meas. Sci. Technol.* **26**(092004) (2015) [doi:10.1088/0957-0233/26/9/092004].

[5] N. Lagakos and R. Mohr, "Stress optic coefficient and stress profile in optical fibers," *Appl. Opt.* **20**(13), 2309–2313 (1981).

[6] A. Bertholds and B. Dändliker, "Determination of the individual strain-optic coefficients in single-mode optical fibers," *J. Light. Technol.* **6**(n°1), 17–20 (1988).

[7] Chu and Whitbread, "Measurement of stresses in optical fiber and preform," *Appl. Opt.* **21**(23), 4241–4245 (1982).

[8] S. Acheroy, P. Merken, H. Ottevaere, T. Geernaert, H. Thienpont, and F. Berghmans, "Influence of measurement noise on the determination of the radial profile of the photoelastic coefficient in step-index optical fibers.," *Appl. Opt.* **52**(35), 8451–8459 (2013).

[9] S. Acheroy, M. Patrick, G. Thomas, H. Ottevaere, H. Thienpont, and F. Berghmans, "On a possible method to measure the radial profile of the photoelastic constant in step-index optical fiber," in *Opt. Sens. Detect. III*, F. Berghmans, A. G. Mignani, and P. De Moor, Eds., Proc. of SPIE Vol. 9141, 914115 (2014) [doi:10.1117/12.2050343].

[10] C. C. Montarou, "Residual stress profiles in optical fibers determined by the two-wave-plate-compensator method," *Opt. Commun.* **265**, 29–32 (2006).

[11] G. Pretzler, H. Jäger, T. Neger, H. Philipp, J. Woisetschläger, N. Co-investigator, E. González-Ramírez, E. de la Rosa Miranda, J. G. Arceo-Olague, et al., "Comparison of different methods of abel inversion using computer simulated and experimental side-on data," *Natuforschung* **47a**(April 23), 955–970 (1992) [doi:10.1017/CBO9781107415324.004].

[12] S. Acheroy, P. Merken, H. Ottevaere, T. Geernaert, H. Thienpont, and B. Francis, "Influence of measurement noise on the determination of the radial profile of the photoelastic coefficient in step-index optical fibers," *Appl. Opt.* **52**(35), 8451–8459 (2013).

[13] K. Tatekura, "Determination of the index profile of optical fibers from transverse interferograms using Fourier theory," *Appl. Opt.* **22**(3), 460–463 (1983).

[14] H. Poritsky, "Analysis of thermal stresses in sealed cylinders and the effect of viscous flow during anneal," *Physics (College. Park. Md).* **5**, 406–411 (1934).

[15] M. R. Hutsel and C. Montarou, "Algorithm performance in the determination of the refractive-index profile of optical fibers," *Appl. Opt.* **47**(6), 760–767 (2008).

[16] T. Chartier, C. Greverie, L. Selle, L. Carlus, G. Bouquet, and L.-A. de Montmorillon, "Measurement of the stress-optic coefficient of single-mode fibers using a magneto-optic method.," *Opt. Express* **11**(20), 2561–2566 (2003) [doi:10.1364/OE.11.002561].

[17] G. Pretzler, H. Jäger, T. Neger, H. Philipp, and J. Woisetschläger, "Comparison of Different Methods of Abel Inversion Using Computer Simulated and Experimental Side-On-Data," *Zeitschrift für Naturforschung. A, A J. Phys. Sci.* **47**(9), 955–970 (1992).

[18] L. V. Fausset, *Applied numerical analysis using Matlab*, M. Horton, Ed., Prentice Hall (1999).

[19] "www.thorlabs.de."

[20] T. Z. N. Sokkar, W. A. Ramadan, M. A. Shams El-Din, H. H. Wahba, and S. S. Aboleneen, "Bent induced refractive index profile variation and mode field distribution of step-index multimode optical fiber," *Opt. Lasers Eng.* **53**, 133–141 (2014).

[21] "http://fiberguide.com/wp-content/uploads/2013/03/All_Silica_Fiber_0301131.pdf."

[22] W. Primak, "Photoelastic constants of vitreous Silica and its elastic coefficient of refractive index," *J. Appl. Phys.* **30**(5), 779–788 (1959).